Numerical Study on the Effect of Buildings on Temperature Variation in Urban and Suburban Areas in Tokyo

Takayuki TOKAIRIN, Hiroaki KONDO, Hiroshi YOSHIKADO, Yutaka GENCHI, Tomohiko IHARA

National Institute of Advanced Industrial Science and Technology (AIST), Tsukuba, Japan

Yukihiro KIKEGAWA

Meisei University, Tokyo, Japan

Yujiro HIRANO

Gunma University, Kiryu, Japan

and

Kazutake ASAHI

Mizuho Information & Research Institute, Inc., Tokyo, Japan

(Manuscript received 13 October 2005, in final form 3 July 2006)

Abstract

A numerical investigation of the temperature variation in urban and suburban areas due to the presence of buildings was carried out using a one-dimensional canopy model combined with a meso-scale meteorological model. Since temperature increases in an urban area are caused by sensible heat from building surfaces besides anthropogenic heat and reduction of wind speed due to buildings' drag, we estimated each cause separately to determine the contribution by each to the temperature variation. The simulation was performed for Kanda, an urban area, and for Nerima, a suburban area of Tokyo. Comparisons were made with actual temperatures before the estimation. The comparison indicated that the measured temperatures in the Kanda and Nerima areas were nearly reproduced by the model. The sensitivity analysis indicated that, in a comparison with the temperature in no building environment, the contribution of (i) sensible heat flux from building surfaces to temperature rise was 49% in Kanda and 20% in Nerima, (ii) wind reduction due to drag was 41% in Kanda and 59% in Nerima, and (iii) the effect of the interaction between (I) and (II) was +10% in Kanda and +20% in Nerima.

1. Introduction

Urban heat islands (UHIs) frequently occur in large cities. This build-up of heat is detrimental to an urban thermal environment. UHI results in greater energy consumption due to the increased demand for air conditioning in the summer months. Generally, the factors that produce temperature increases due to UHI are (i) anthropogenic heat released from air-conditioning systems and motor vehicles, (ii) sensible heat fluxes from the surfaces of roads and buildings, and (iii) reduction in wind

Corresponding author and present affiliation: Takayuki Tokairin, Department of Environmental Engineering, Building Research Institute, 1 Tachihara, Tsukuba 305-0802, Japan.
E-mail: tokairin@kenken.go.jp

speed, which result in poor ventilation in urban areas. All of these factors contribute to the complexity of assessing their correlations. For this reason, it is difficult to observe and determine the individual contribution of each factor to temperature variation.

Recently, numerical models are being used to study anthropogenic contributions to temperature changes. In one case, Ichinose et al. (1999) quantified the contribution of anthropogenic heat release to UHI and showed that a -0.5°C reduction in temperature by reducing energy consumption for hot water supply and air conditioning. In another case, Ohashi et al. (2005) reported that waste heat from air conditioning produced increases in temperature of 1–2°C on weekdays in the Tokyo business area.

Some studies focused on factors (ii) and (iii) mentioned above were also performed. For example, Kusaka and Kimura (2004) conducted sensitivity experiments to compare the affects on the surface layer air temperature in the urban area using a single layer urban canopy model. This was incorporated into a two-dimensional meso-scale model. The factors they examined were anthropogenic heat, a larger heat capacity due to walls, a smaller sky-view factor due to walls, and a smaller albedo due to walls. They concluded that anthropogenic heating is the most effective to increase surface layer temperature, especially for nocturnal temperature. Although the effect of other factors, specifically the large heat capacity, smaller view factor and a smaller albedo were relatively small for temperature variation, these are not ignorable except for a smaller albedo case.

Martilli (2002) also investigated the relative effect of the thermal and mechanical factors on an urban boundary layer structure using a meso-scale model with an urban surface exchange parameterization. To estimate the effect of each factor on UHI, Martilli (2002) adopted the factor separation technique proposed by Stein and Alpert (1993) (briefly described in later section). One of the results obtained was that, at night, thermal factor was more important for contribution of the UHI formation in a layer near the ground, while the mechanical factor contributes to the inversion strength in the upper layer. Those studies clarified how and how much the factor contributes for UHI formation. However, both studies were made under ideal conditions; virtual urban area was assumed in two-dimensional flat domain.

In this study, evaluation of factors (ii) and (iii) for UHI formation in realistic urban area (Tokyo 23 wards) was performed. To investigate the contribution of each factor, we adopted a combination of a one-dimensional canopy model (hereafter, CM) (Kondo and Liu 1998), and a meso-scale meteorological model (hereafter, MM) (Kondo 1989). For the purpose of model validation, Ohashi et al. (2003) conducted temperature observation in urban areas of Tokyo in 2002. However, since their observation was done only in urban areas, it may be inadequate to validate for the calculation of the whole 23 wards of Tokyo. Therefore, in this study, simultaneous measurements of temperature were carried out at urban and sub-urban areas in Tokyo in July and August 2004, and then comparisons were made with observed temperatures before the estimation.

The structure of this paper is that the model system and CM are introduced in Sections 2 and 3. The model performance is validated using a statistical method in Section 4. In Section 5, a brief description of the field observation, and its results are presented, in addition, comparison of CM results with the observation is also shown. Finally, Section 6 is an estimation of the individual contributions to temperature variation due to reduction of wind speed and sensible heat from buildings in the urban (Kanda) and suburban (Nerima) areas.

2. Framework of the numerical model system

The urban warming phenomenon is generally investigated using a numerical model such as a meso-scale meteorological model. However, meso-scale models are inadequate for analyzing UHIs, because they do not express the influence of the radiative process and drag force of buildings on the variations in temperature. Therefore, another meteorological model, one that functions on the scale of city blocks, is required to treat these specific effects. In this study, these effects are considered in CM connected with MM. Figure 1 illustrates the model system. In the MM, Grid Point Value data provided by the Japan Meteorological Agency (JMA 2002) was used. The GPV data is obtained from

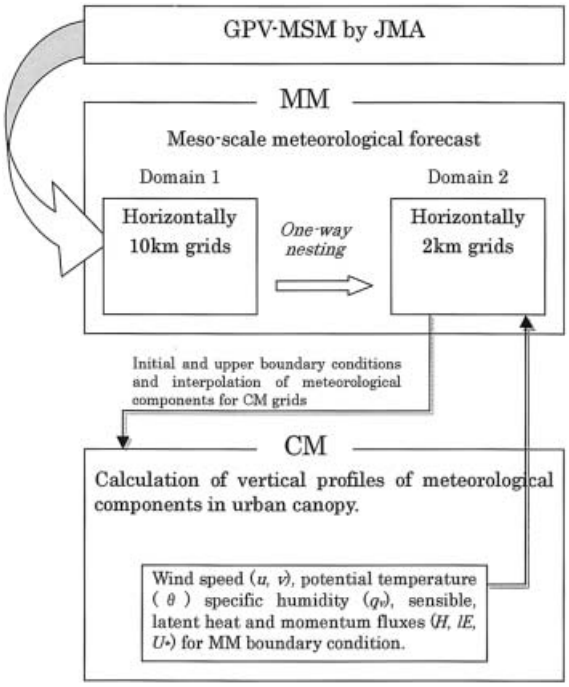

Fig. 1. Simulation system consists of two models (MM and CM). In the MM, two types of computational domains are considered (outer domain: Domain 1 and inner domain: Domain 2). Domain 1 covers most of the central part of Japan. The nested region (Domain 2) covers the whole Kanto district (see Fig. 3). One CM is connected with one MM grid. The CM receives initial and upper boundary conditions from the MM, and returns calculated results to the MM (two-way nesting).

Grid Point Value Meso Scale Model (GPV-MSM), which is one of the numerical weather prediction models and provides the predicted value of meteorological components for each grid point of an outer computational domain in MM (Domain 1 in Fig. 1). One-way nesting was adopted to propagate meteorological information for an inner domain (Domain 2 in Fig. 1). One CM is connected with one MM grid. CM receives initial and upper boundary conditions from MM and returns calculated results to MM (two-way nesting).

3. Brief description of CM

In this section, we briefly describe the CM used in this study. The basic equations of the CM are presented below.

$$\frac{\partial u}{\partial t} = \frac{1}{m}\frac{\partial}{\partial z}\left(K_m \cdot m \cdot \frac{\partial u}{\partial z}\right) - cau(\sqrt{u^2+v^2}) + F_u \quad (1)$$

$$\frac{\partial v}{\partial t} = \frac{1}{m}\frac{\partial}{\partial z}\left(K_m \cdot m \cdot \frac{\partial v}{\partial z}\right) - cav(\sqrt{u^2+v^2}) + F_v \quad (2)$$

$$\frac{\partial \theta}{\partial t} = \frac{1}{m}\frac{\partial}{\partial z}\left(K_h \cdot m \cdot \frac{\partial \theta}{\partial z}\right) + \frac{Q_{AS}}{c_p \rho} \quad (3)$$

$$\frac{\partial q_v}{\partial t} = \frac{1}{m}\frac{\partial}{\partial z}\left(K_q \cdot m \cdot \frac{\partial q_v}{\partial z}\right) + \frac{Q_{AL}}{l\rho} \quad (4)$$

where u and v are the wind velocity components for the x (toward east for positive) and y (toward north for positive) directions. θ, q_v, Q_{AS}, and Q_{AL} denote the potential temperature, specific humidity, anthropogenic sensible heat, and anthropogenic latent heat, respectively. The turbulent diffusion coefficients (K_m, K_h, and K_q) in Eqs. (1) to (4) are obtained from Gambo's (1978) formula. F_u and F_v denote Coriolis parameters. a and m are defined below:

$$m = 1 - \frac{b^2}{(b^2+w^2)} \cdot P_w(z) \quad (5)$$

$$a = \frac{b \cdot P_w(z)}{(b+w)^2 - b^2 \cdot P_w(z)} \quad (6)$$

where b, w and $P_w(z)$ stand for the width of a building, the distance between buildings and the building floor density distribution at height z as obtained from the GIS data. In Eq. (5), m corresponds to the volume porosity of one urban block, shown in Fig. 2. a in Eq. (6) denotes building surface area per unit volume.

The surface heat budget is considered for the ground, roof, and building walls at each level. In the CM, the building walls consist of four surfaces that precisely face north, south, east, and west. An equation of the heat budget on the surfaces is described below.

$$c_w \rho_w \frac{\partial T_w}{\partial t}\delta = R_N + Q + lE + G \quad (7)$$

where c_w and ρ_w are the heat capacity and density for the building wall, roof, or ground, respectively, T_w is the surface temperature of the wall, roof, or ground, δ is the thickness of the

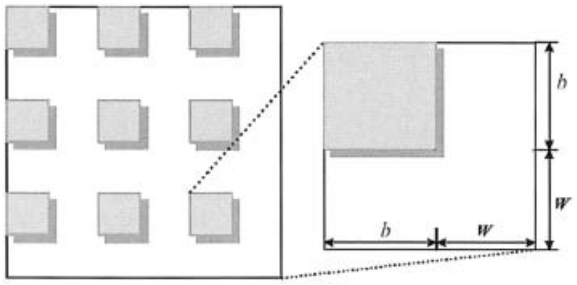

Fig. 2. Illustration of building's configuration assumed in the CM. In the model, the building is arranged at equal intervals. The width of the building and road, are represented in b and w, respectively.

first layer, and R_N, Q, lE, and G are the net radiative flux, sensible and latent heat fluxes, and heat storage in a building wall, respectively. When the surface temperature is higher than air-temperature, sensible heat flux Q is obtained as follows (Jurges 1924):

$$Q = \alpha(T_w - T_a) \tag{8}$$

where T_a is air-temperature and

$$\alpha = \begin{cases} 6.15 + 4.18U & U \leq 5(ms^{-1}) \\ 7.51U^{0.78} & U > 5(ms^{-1}) \end{cases} \tag{9}$$

Monin-Obukhov theory is used for sensible heat flux as $T_w < T_a$, and momentum flux on surfaces (Kondo 1994). For the latent heat, plant canopy conductance is introduced:

$$\frac{E}{\rho} = \left(\frac{G_a G_S}{G_a + G_S}\right)[q_{vS}(T_S) - q_v(T_a)] \tag{10}$$

where G_a is the aerodynamic conductance, G_S, the plant canopy conductance and $q_{vS}(T_S)$, the saturated specific humidity at T_S. Heat storage G is represented as follows:

$$G = -c_w \rho_w K_w \frac{\partial T_w}{\partial n} \tag{11}$$

where $\partial/\partial n$ and K_w denote the derivative perpendicular to the surface, and thermal diffusivity. T_w is calculated from a one-dimensional thermal conduction equation:

$$\frac{\partial T_w}{\partial t} = \frac{\partial}{\partial n}\left(K_w \frac{\partial T_w}{\partial n}\right) \tag{12}$$

The radiation process in an urban canopy is the most complicated physical phenomenon to treat in a numerical model. In the CM, directed, diffused, and reflected solar insolation from surfaces are considered; however, since the reflection process in an urban canopy is so complicated, the CM deals with the reflection from surfaces only once. Details of the model are described in a paper by Kondo et al. (2005).

4. Model validation using a statistical method

4.1 Methodology

For a quantitative validation of model performance, Keyser and Anthes (1977) proposed the following relationship:

$$\sigma \fallingdotseq \sigma_{obs} \tag{13}$$

$$E < \sigma_{obs} \tag{14}$$

$$E_{UB} < \sigma_{obs} \tag{15}$$

where σ and σ_{obs} denote the standard deviation of the calculation and observation results, respectively. E and E_{UB} stand for the root mean square error and the unbiased root mean square error. E_{UB} is obtained from E corrected by the averaged bias between the calculation and the observation. Kikegawa (2001) applied this evaluation procedure to the potential temperature and wind speed calculated by the MM and evaluated the model performance quantitatively. Willmott (1982) introduced a following indicator, named "Index of Agreement (IA)":

$$IA = 1 - \frac{\sum_{i=1}^{N}(P_i - O_i)^2}{\sum_{i=1}^{N}(|P_i'| + |O_i'|)^2} \tag{16}$$

where P_i and O_i are the model-predicted and observed quantities at the i^{th} measurement site, respectively. P_i' and O_i' are given as $P_i' = P_i - \bar{O}$, and $O_i' = O_i - \bar{O}$ ($\bar{O}$: averaged observation result). IA varies between 0 and 1; $IA = 1$ corresponds to the perfect simulation. In the present study, we also adopted these methods to evaluate the calculation results of the MM and CM.

4.2 The MM and CM performance

Because CM combined with the MM is affected by meso-scale meteorological condition, the MM model performance is first examined in comparison with AMeDAS (Automated Meteorological Data Acquisition System by the

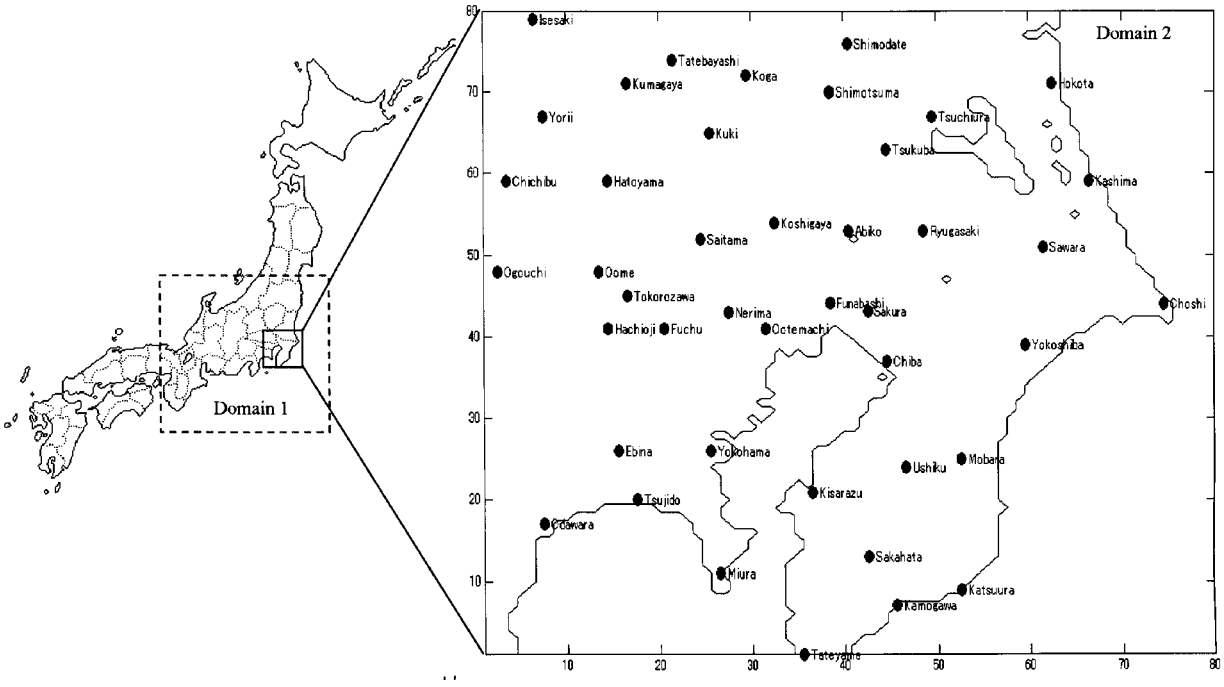

Fig. 3. Calculation domain for the MM (dotted square: Domain 1). In the right figure (Domain 2), 43 AMeDAS sites are illustrated. Note that 'Ootemachi' site represents the Kanda area.

Japan Meteorological Agency) data. In the present study, 43 AMeDAS sites in the computational domain of MM were selected (see Fig. 3). The simulation period for the validation was 37 hours (from 0:00 a.m. on 27 July to 12:00 p.m. on 28 July, 2004 (JST)), which includes our observation period. The number of samples, therefore, is 1,591 (37 hours by 43 sites of AMeDAS) in MM validation. For solar radiation, MM had originally adopted Kondo's (1994) formula, corrected with data concerning cloud amount provided by the JMA GPV-MSM. However, since the predicted cloud amount is sometimes overestimated, the calculated insolation in MM tends to be lower than what is observed ('Ins0' in Fig. 4). We, therefore, introduced that solar radiation is calculated from the hourly sunshine rate provided by AMeDAS sites (Yoshikado 1991) ('Ins1' in Fig. 4).

CM performance was also evaluated with the same method and the same simulation period. Since hourly temperature and wind speed are recorded only at Kanda and Nerima AMeDAS in the Tokyo 23 wards, the number of sample is 74 (37 hours by 2 sites of AMeDAS).

Table 1-1 shows the results of the MM validation for the temperature and absolute wind velocity. In this table, the correlation coefficient (r) and Index of Agreement (IA) for the temperature are 0.89 and 0.93, respectively. The computed results also satisfy conditions (8) to (10). This suggests that the MM performance is reasonable statistically for temperature calculation in the meso-scale level. On the other hand, the performance of MM for wind speed was lower than that of temperature. However, Kikegawa (2001) reported that Pielke and Marher (1978) also obtained $E_{UB}/\sigma_{obs} = 1.0$ to 1.4 using the Colorado State University Meso-scale Model (CSUMM) for wind calculation, and IA in Otte et al. (2004) was 0.5 to 0.6 obtained from the MM5 calculation result. This suggests that the performance of the MM used in this study was as accurate as that of other meso-scale models.

The result of CM validation is shown in Table 1-2. Compared to the results of MM performance (Table 1-1), CM performance is fairly improved in both temperature and wind speed.

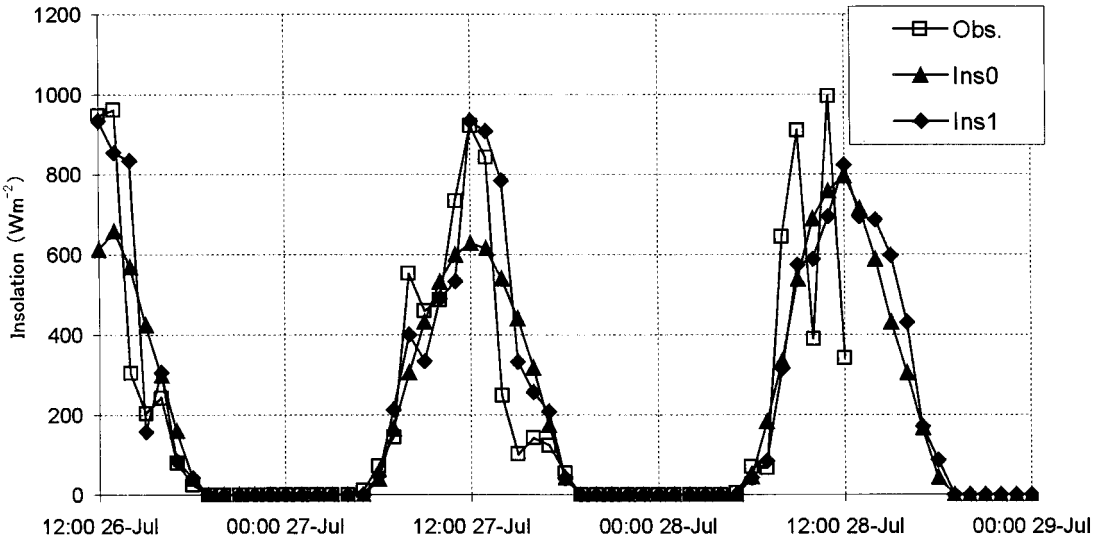

Fig. 4. Comparison between the insolation that is calculated by two different ways ('Ins0' and 'Ins1'), and observed at the roof of the building in Kanda ('Obs'). In 'Ins0', the peak of insolation is lower than 'Obs', due to overestimation of predicted cloud amount given by GPV-MSM. On the other hand, 'Ins1' is well reproduced at the peak. Solar insolation in 'Ins 1' is obtained from the hourly sunshine rate, by AMeDAS.

Table 1-1. Result of validation for the MM

	No. of sample	Averaged bias	E	E_{UB}	σ	σ_{obs}	r	IA
Temp. (°C)	1591	0.05	1.44	1.02	2.50	3.13	0.89	0.93
Wind (ms^{-1})	1591	0.25	1.37	1.15	1.13	1.39	0.47	0.67

Table 1-2. Result of validation for the CM

	No. of sample	Averaged bias	E	E_{UB}	σ	σ_{obs}	r	IA
Temp. (°C)	74	0.67	0.83	0.49	2.52	2.77	0.99	0.98
Wind (ms^{-1})	74	−0.17	0.93	0.91	1.40	1.58	0.87	0.91

5. Comparison of CM result with observation data in Tokyo

5.1 Methodology of the field observation

As stated previously, simultaneous measurements of daily temperature variations were carried out at two locations in Tokyo. The observation method we adopted was proposed by Ohashi et al. (2003). The areas selected were the Kanda and Nerima districts (see Fig. 5). Kanda, an urban area near Tokyo Bay, is a business district with many office buildings, and Nerima, a suburban inland area, is a residential district. The 24-hour observation was carried out twice at each location. The first observation began at 12:00 on 27 July (JST), and the second, at 12:00 on 7 August 2004 (JST). Figure 6a, b illustrates the observation areas and measurement points. The size of each domain is approximately 200 × 300 m square. In these areas, more than ten measurement points indicated in the maps were set, and we recorded the air and ground surface temperatures, and motor traffic volume at 30-minute intervals. At each point, traffic volumes were counted for one minute and the air tempera-

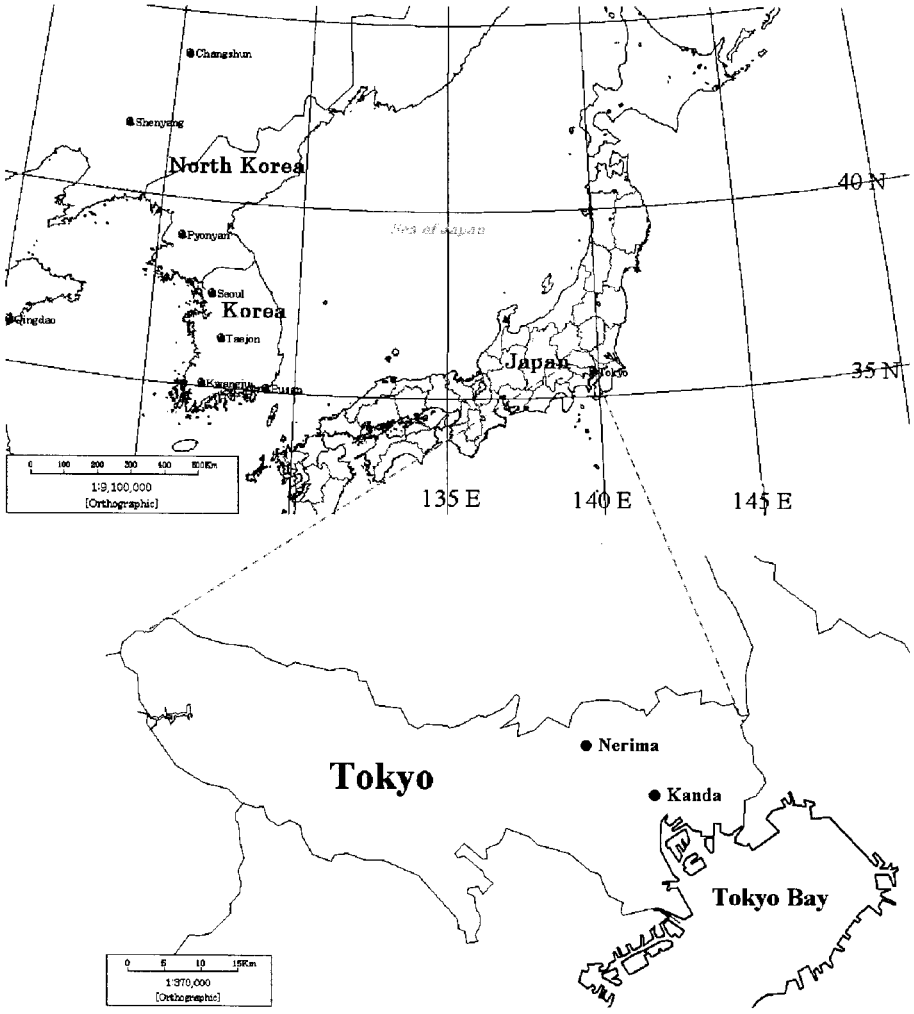

Fig. 5. Locations for field observation in Tokyo. Kanda area (a business district) is close to Tokyo Bay and Nerima area (a residential district) is located relatively inland.

ture was measured approximately 1.5 m above the ground. In addition, the wind speed, wind direction, and solar radiation were measured at the roof of a building in Kanda, and at the terrace of a house in Nerima.

5.2 Comparison between observed temperatures in July

Figure 7 shows the daily temperature variations during the observation in July, averaged over all the observation points in both areas. In the figure, solid and dotted lines denote the temperatures in Kanda and Nerima, respectively. During the observation, the maximum temperatures were about 35°C in both areas. From afternoon to early morning, the average temperatures decreased, and the recorded minimum occurred at approximately 4 a.m. in both areas. Figure 7 also shows that the temperature in Kanda is slightly higher from late afternoon to early morning. The maximum temperature difference between both observation areas was also seen at around 4:00 on 28 July (about 1°C higher in Kanda). Mikami et al. (2004) and Ando et al. (2003) also obtained similar results from their long-term observations, that is, a UHI appears from midnight to early morning in the center of Tokyo, including the Kanda area, and then it moves further inland from morning to mid-afternoon.

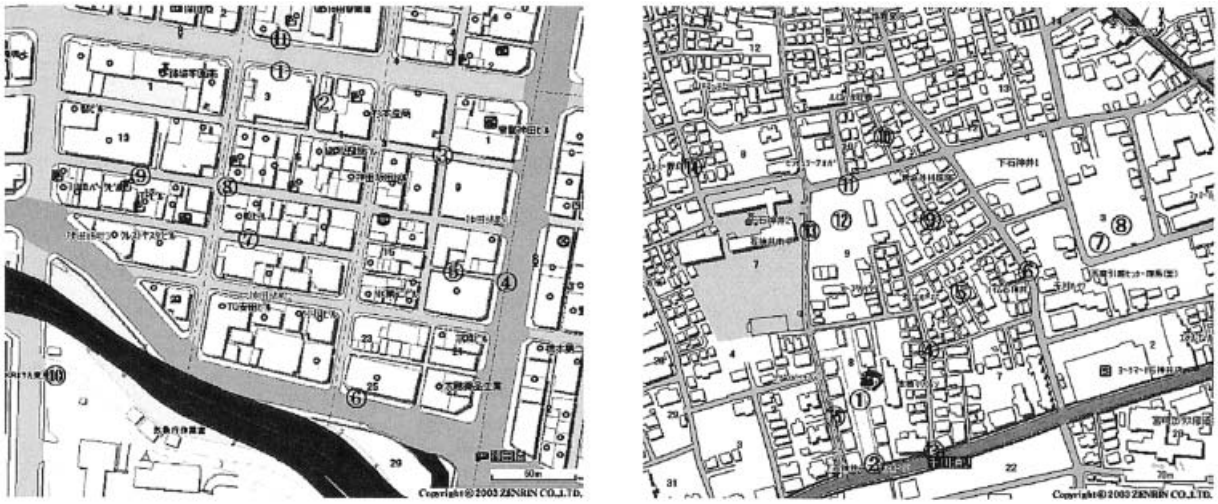

Fig. 6. Observation areas. Numbers in both maps indicate measurement point. Land cover is asphalt in Kanda for all measurement points. On the other hand, land cover in Nerima is asphalt, grass (No. 8, 12) and soil (No. 7). In the Kanda area, AMeDAS site is located at No. 10 (the map software 'ZENRIN Z6' was used).

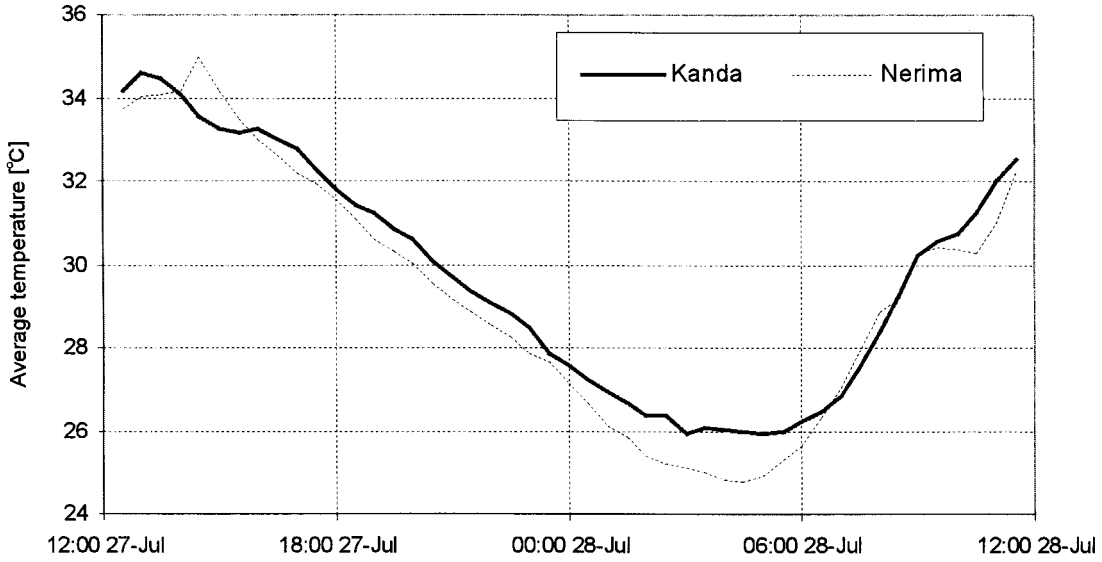

Fig. 7. Averaged daily temperature variations in Kanda (solid line) and Nerima (dotted line) districts during July observation. Daytime temperature tends to be higher in Nerima, while temperature in nighttime is higher in Kanda. The greater difference between Kanda and Nerima is seen from night to early morning.

5.3 CM settings

As can be seen in Fig. 1, CM is combined with MM by two-way nesting to calculate the meteorological components in and above the urban canopy. Kondo et al. (2005) applied the CM to 9 grids, which included Tokyo business district that meteorological observation was performed in 2002. Their simulation result showed that predicted nighttime temperature was lower than observed temperature and thus,

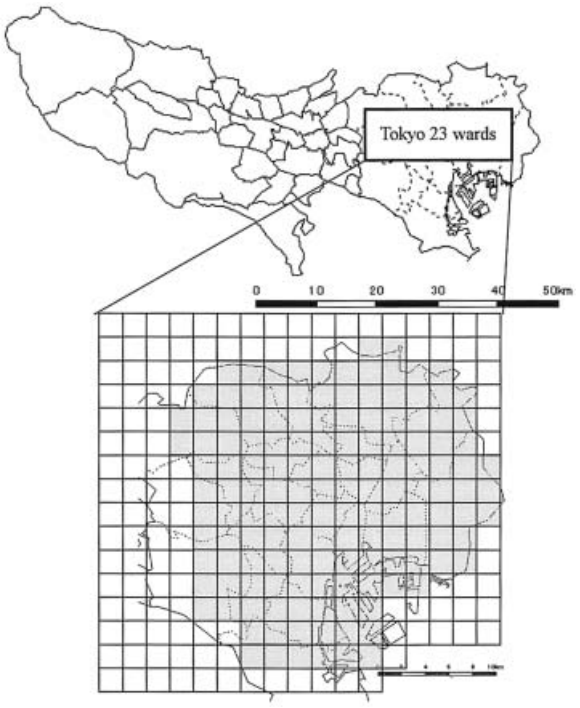

Fig. 8. The CM applied grids (shaded part). The size of a grid is approximately 2 km horizontally.

they concluded that '9 grid' simulation may be inadequate for evaluating the entire urban thermal environment of Tokyo. Therefore, in this study, the CM is applied to grids that cover 23 of the Tokyo wards (Fig. 8). As a result, the number of grids to which the CM is applied is 145. In this sub-section, the calculated results obtained by the CM are compared with the July observation results. The height of calculated temperature is 1 m above the ground. The number in the legend of Figs. 9 and 11 indicates the location of the measurement points shown in Fig. 6a, b. As mentioned in Section 2, one CM is connected with one grid of the MM, which is about 2 km $\times$ 2 km square. Table 2 shows the model parameters used in the CM. In the present simulation, the wall material is assumed to be concrete in the urban area, including Kanda, and heat insulator in the suburban areas, such as Nerima.

5.4 The Kanda area

Figure 9 is a comparison of the calculated and observed temperatures. The scattering of the observed data (symbols) shows that the distribution of the daytime temperature was inhomogeneous due to the presence of sun and shade, while temperature at nighttime did not differ remarkably among the measurement points. The results also show that, throughout the observation period, the temperature at each measurement point was higher than that measured by AMeDAS. The reason is that meteorological instruments for AMeDAS are usually installed above the grass in open areas, and therefore, the instruments are not significantly influenced by anthropogenic heat, sensible heat from buildings and grounds covered with artificial materials. In contrast, since the measurements in this study were done in a densely urban area, released heat from buildings and roads strongly contribute temperature rise. Simulation results obtained by both CM and MM are indicated that CM better reproduces the daytime temperature. In nighttime, calculated temperature by CM results in a similar level of the observation, while '9 grid' simulation by Kondo (2005) indicated that calculated result was lower than observed result. As stated in our introduction, anthropogenic heat was not considered in this time. Therefore predicted results in nighttime should be slightly smaller than observed results.

Table 2. Model parameters for CM. 'W', 'G' denote 'Wall' and 'Ground'

	Average building width w [m]	Average distance between buildings b [m]	Volumetric heat capacity ($\times 10^6$) [$Jm^{-3}K^{-1}$]	Density ρ ($\times 10^3$) [kgm^{-3}]	Thickness of the first layer δ [m]	Thermal conductivity [$Jm^{-1}s^{-1}K^{-1}$]
Kanda (urban)	14.7	13.6	2.01 (W) 2.01 (G)	2.01 (W) 2.01 (G)	0.0133	2.28 (W) 0.73 (G)
Nerima (sub-urban)	10.1	7.9	0.60 (W) 2.01 (G)	0.50 (W) 2.01 (G)	0.0133	0.03 (W) 0.73 (G)

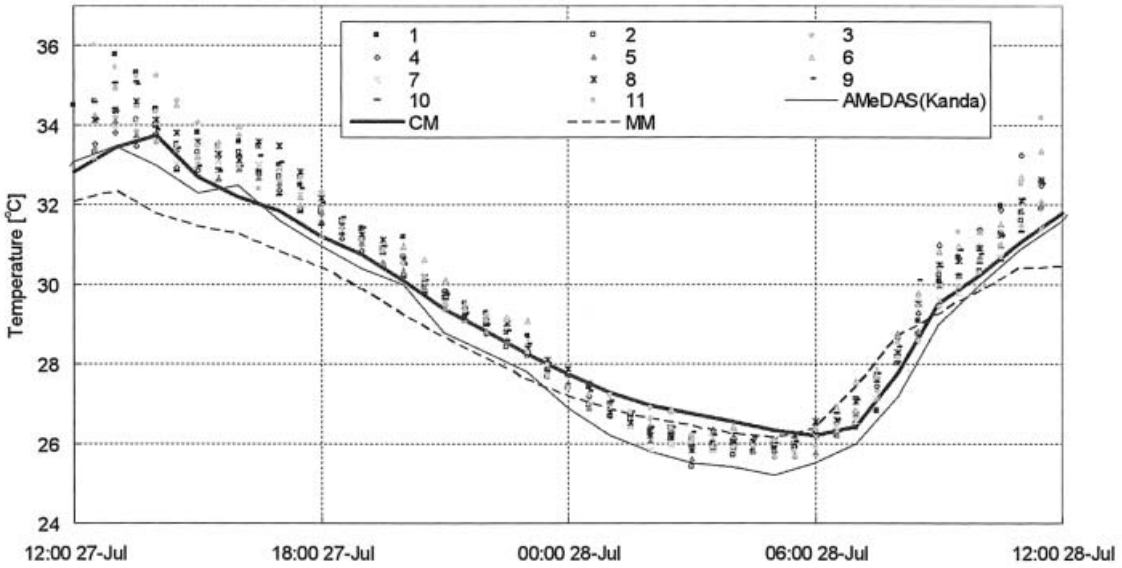

Fig. 9. Comparison between observed and calculated temperatures (MM and CM). AMeDAS data is also added. Observed temperature is higher than that measured at the AMeDAS site. Measurement height at the AMeDAS is 1.5 m above the ground.

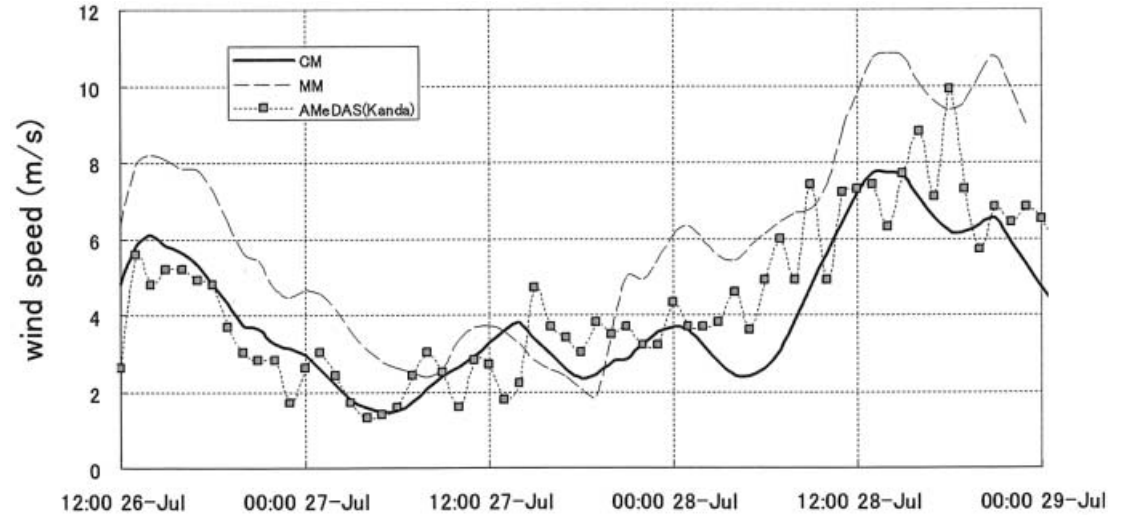

Fig. 10. Comparison of absolute wind speed between the AMeDAS, and calculation by the CM and the MM. Note that the wind speed of AMeDAS is measured at 75 m high.

Figure 10 shows the variation of absolute wind speed observed by AMeDAS (Kanda area: square symbol) and simulated by MM and CM. The anemometer of AMeDAS is installed approximately 75 m above the ground (top of the building), and the calculated results correspond to the same height of AMeDAS. As shown in Fig. 10, MM tends to overestimate observed wind speed. On the other hand, calculation by CM is good agreement with the observation.

5.5 The Nerima area

Figure 11 shows the same as Fig. 9 except for the Nerima area. In this figure, observed

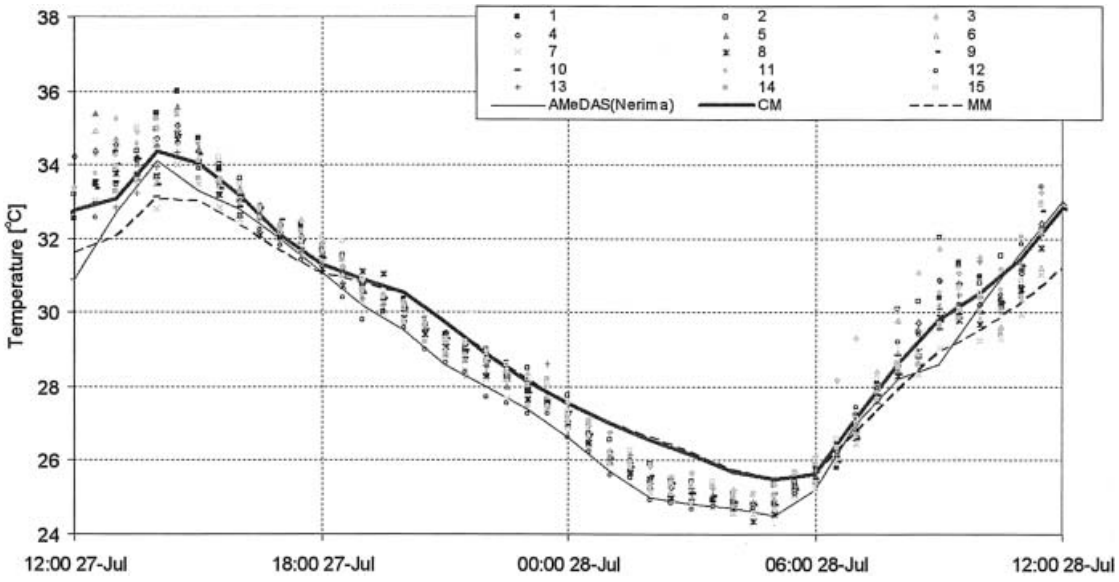

Fig. 11. Same as Fig. 9, but for the Nerima area. Calculation by the CM well reproduces observed temperature during daytime, while calculated result in the nighttime is slightly overestimated. Measurement height at the AMeDAS is 1.5 m above the ground.

temperature in daytime is also widely scattered. However, the difference between our observations and the AMeDAS temperature is smaller than that in Kanda, even though the distance between the Nerima site of AMeDAS and our observation area (Nerima) is approximately 6 km. This is because that the urban structure around the AMeDAS site at Nerima is similar to that at the observation area. The CM performance for daytime temperature is also better than MM. However, CM slightly overestimates the nighttime temperature. On the other hand, the calculation of the wind speed shows the similar tendency of the observations by AMeDAS (Fig. 12). Note that the wind speed is recorded as an integer value at the Nerima AMeDAS.

6. Contribution to the temperature variation due to buildings

6.1 Simulation cases

Wind reduction due to the drag of the buildings and storage of heat in the urban canopy are the major causes of urban warming except for anthropogenic heat discharge. To estimate the contribution of these two effects to temperature variation, four simulations, shown in Table 3, were conducted. They included (a) Case0 (control run): realistic situation that is already shown as the calculated results in Fig. 9 (Kanda) and Fig. 11 (Nerima), (b) Case1: Only thermal effects (sensible heat flux and radiation from the building walls and roofs) of buildings are considered. Buildings do not exist for wind, that is, no drag due to buildings is considered. (c) Case 2: Only drag effect of building on wind is considered. Neither heat flux nor radiation from the building walls is given. (d) Case 3: The drag, heat flux, and radiation from the building walls are not considered; that is, no buildings in the entire 23 wards of Tokyo are presented.

It is important to point out that only sensible heat flux from the ground is considered in all cases, and anthropogenic heat for the CM-applied grids is not considered in this study. The simulation period was from 12:00 on 26 July to 0:00 on 29 July (JST).

6.2 Factor separation

To estimate the contribution of factors for UHI, Martilli (2002) adopted a simple factor separation method proposed by Stein and Alpert (1993). According to Stein and Alpert (1993), interaction among factors should not be neglected for sensitivity analysis and thus, 2^n

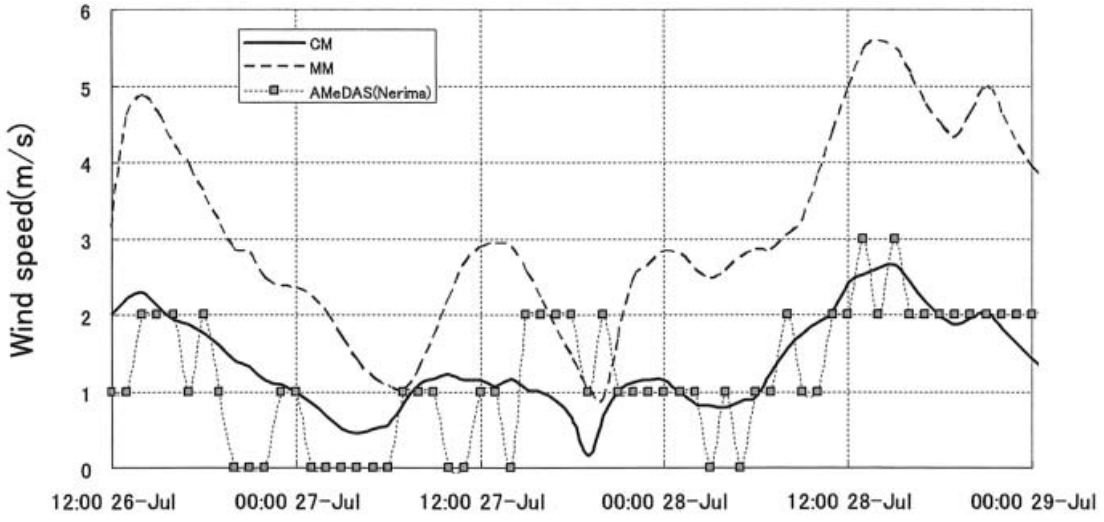

Fig. 12. Same as Fig. 10, but for the Nerima area. Wind speed is measured at 6 m above the ground at the AMeDAS site. Note that observed wind speed, is given as an integer value.

Table 3. Simulation cases

	Case0	Case1	Case2	Case3
Wind reduction by drag of buildings	On	Off	On	Off
Heat release from building surfaces	On	On	Off	Off

simulations are required to evaluate the contribution of n factors. We applied the method to our simulation cases:

$$\hat{c}_3 = \text{Case3} \tag{17}$$

$$\hat{c}_1 = \text{Case1} - \text{Case3} \tag{18}$$

$$\hat{c}_2 = \text{Case2} - \text{Case3} \tag{19}$$

$$\hat{c}_{12} = \text{Case0} - (\text{Case1} + \text{Case2}) + \text{Case3} \tag{20}$$

where Case0 to 3 denotes temperature. $\hat{c}_1$, $\hat{c}_2$ and $\hat{c}_{12}$ are the effect of sensible heat release from building surfaces, wind reduction due to drag and those interaction, respectively.

6.3 *Simulation results*

Figures 13 and 16 show simulated temperature variations in Kanda and Nerima. In both areas, a similar tendency can be seen, that is, temperature among all cases is not largely scattered in the morning. The reason is that the amount of released sensible heat is larger in Case 1 and 3, since wind speed in Case 1 and 3 (no drag condition) is larger than in other cases. Therefore, temperature increases in Case 1 and 3 is faster than that in Case 0 and 2. As a result, temperature differences among cases become small in the morning. On the other hand, from afternoon to the next early morning, differences are clearly visible. In this period, the relative impact of sensible heat from building surfaces (Case1), wind reduction due to drag (Case2), and interaction (Int.) between Case1 and 2 was evaluated with the factor separation method previously mentioned. Through a comparison with Case3 (No buildings exist) in the Kanda area, the average temperature increase is 1.02°C in Case0, 0.50°C in Case1, 0.42°C in Case2 and 0.10°C in interaction between Case1 and Case2 (Fig. 13). Sensible heat flux from surfaces and averaged surface temperatures are also shown in Figs. 14 and 15. In Case1, no drag results in the increase of the wind speed, therefore, the amount of released sensible heat is also relatively large (Case1 in Fig. 14). However, from afternoon to the next early morning, temperature is lower than that in Case0 due to the large advection and lower

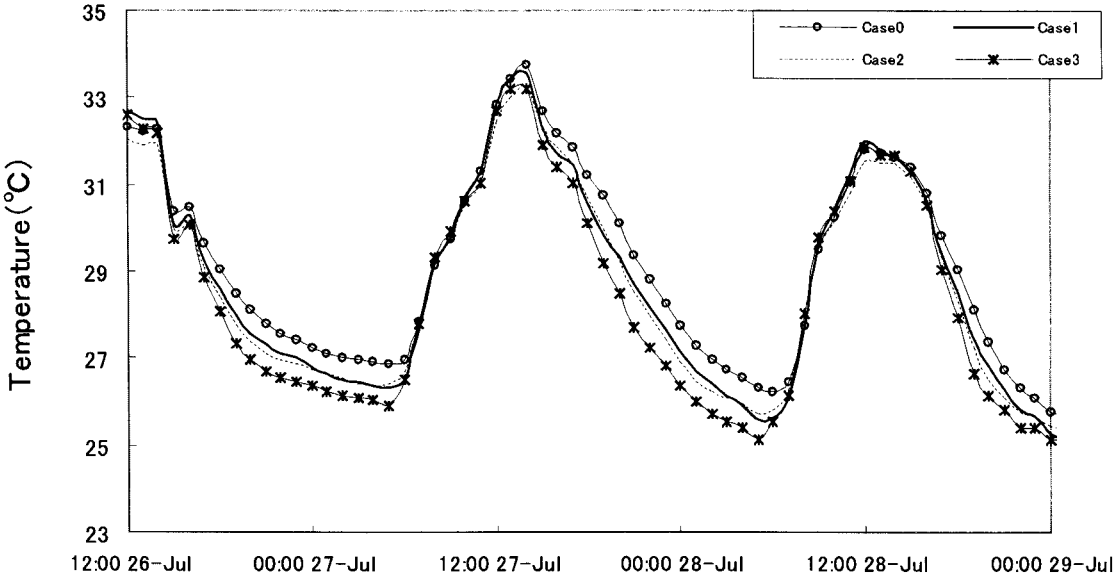

Fig. 13. Calculated temperature variations for all cases in the Kanda area. The difference among the cases appeared from every afternoon, to early morning.

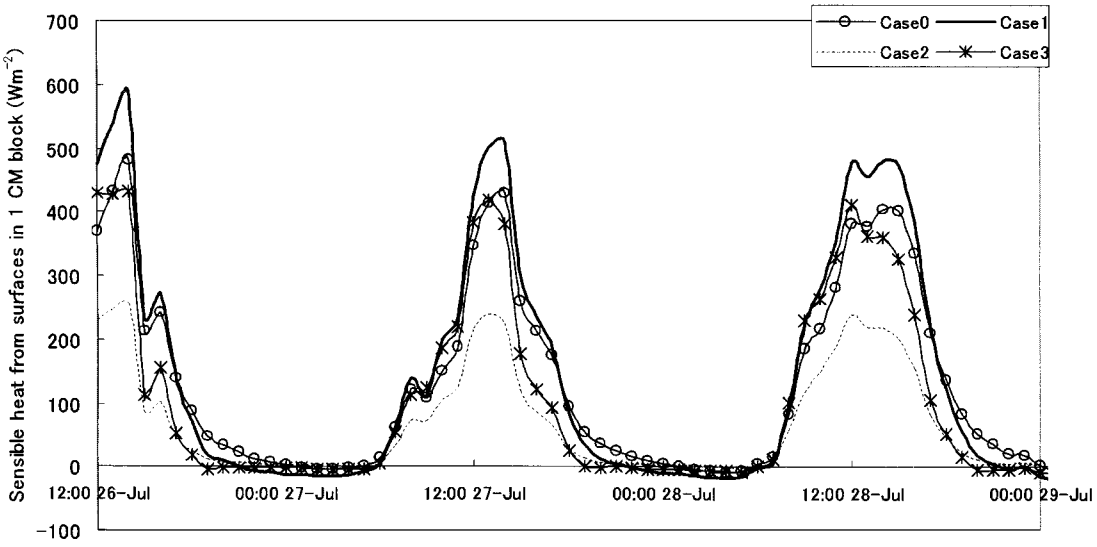

Fig. 14. Calculated sensible heat in all cases. Sensible heat is released from building walls, roof and ground in Case 0 and Case1. On the other hand, it is released from only ground in Case 2 and Case 3.

surface temperature (Case1 in Fig. 15). In Case2, sensible heat is released exclusively from the ground, that is, no heat exchange between building surfaces (walls and roofs) and atmosphere, and no shade nor no long wave radiation from building surfaces are considered. As a result, surface temperature in Case2 has the highest peak among all cases (Case2 in Fig. 15).

On the other hand, in the Nerima area, the

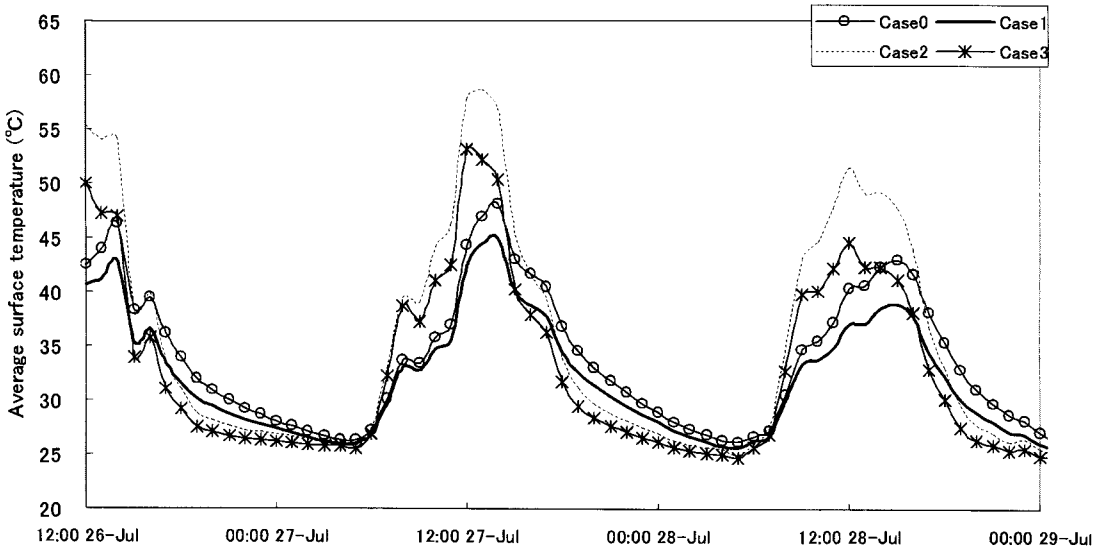

Fig. 15. Variation of averaged surface temperature (averaged over all surfaces: walls, roof and ground in Case 0 and 1: only ground in Case 2 and 3).

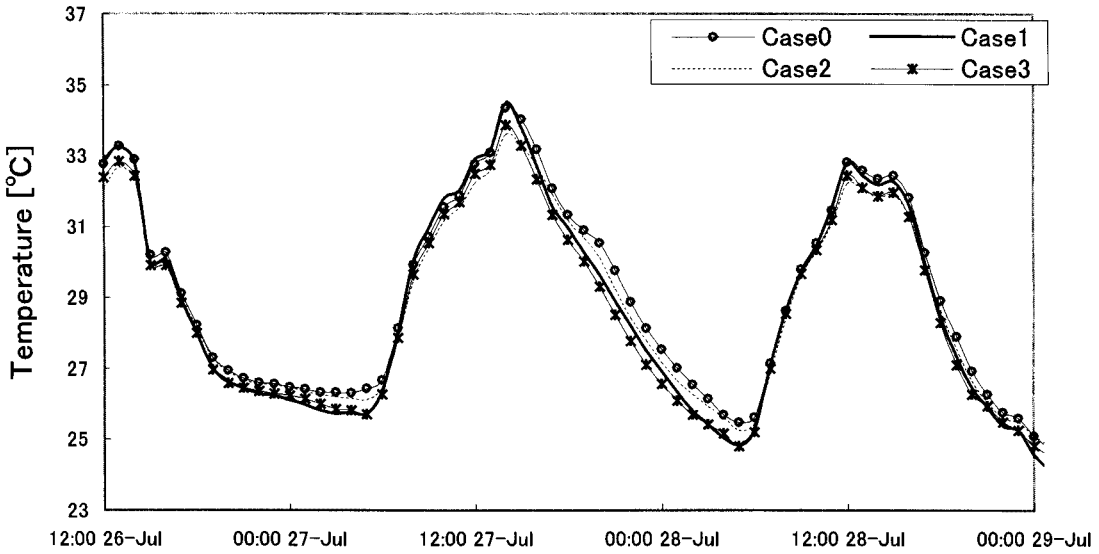

Fig. 16. Same as Fig. 13, but for the Nerima area. The same tendency of temperature variation in Kanda was obtained. Contribution to temperature increase by considering only sensible heat release (Case1), is relatively lower than that by only considering the reduction of wind speed (Case2) during nighttime.

average temperature increase is 0.58°C in Case0, 0.12°C in Case1, 0.34°C in Case2, and 0.12°C in the interaction. The temperature difference between Cases 0 and 3 is smaller (0.58°C) than that reported in Kanda (1.02°C). The difference of surface temperature among cases is also smaller than that in Kanda (Fig. 18). The reason is that, as shown in Fig. 17, the amount of released sensible heat from buildings in Nerima is smaller than that re-

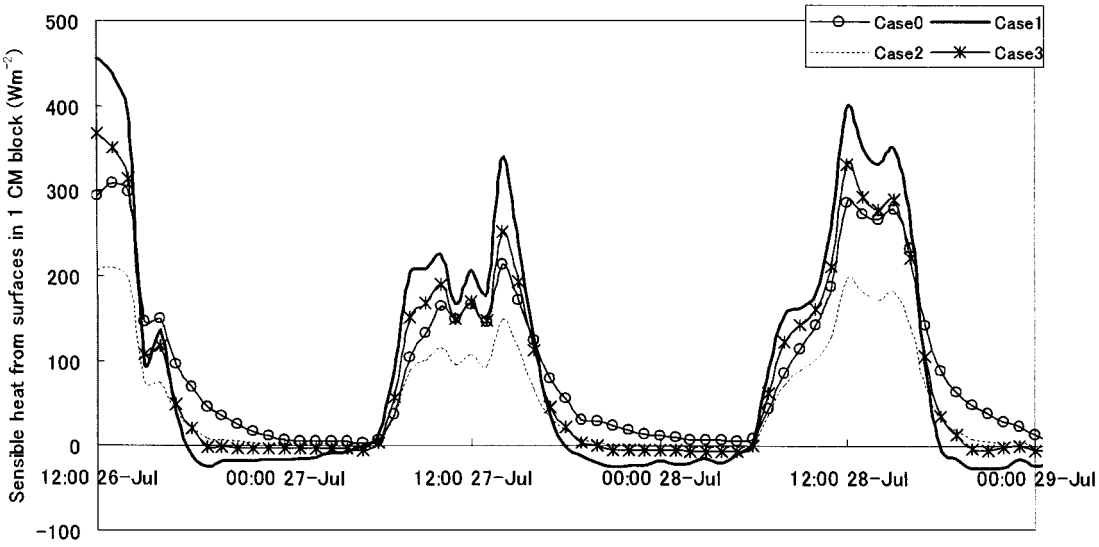

Fig. 17. Same as Fig. 14, but for the Nerima area.

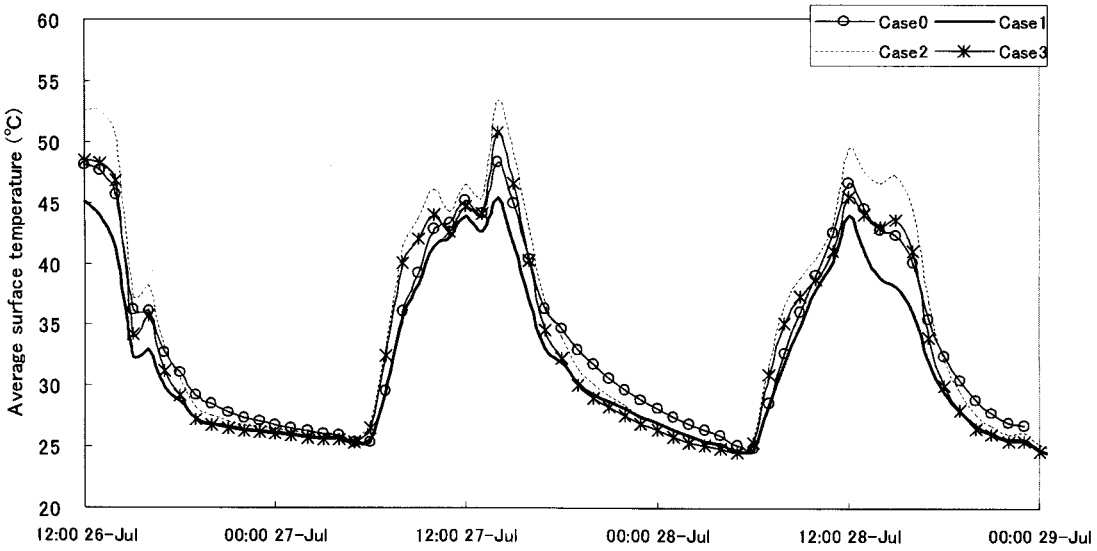

Fig. 18. Same as Fig. 15, but for Nerima.

ported in Kanda due to the difference in the building surface area and thermal properties of the wall material- such as the heat capacity and thermal conductivity (Table 2).

Figure 19 shows the contribution of each factor in both Kanda and Nerima. In the Kanda area, contribution of sensible heat release from buildings (Case1) for temperature rise is slightly higher (49%) than that of wind reduction (Case2) due to drag (41%), while wind reduction (Case2) is dominant in the Nerima area, that is, because sensible heat release from building surfaces is relatively small in Nerima, the effect of wind speed is relatively significant. The contribution of their interaction ('Int.' in Fig. 19) in Kanda is smaller (10%) than other factors. However, Nerima is not ignorable (20%).

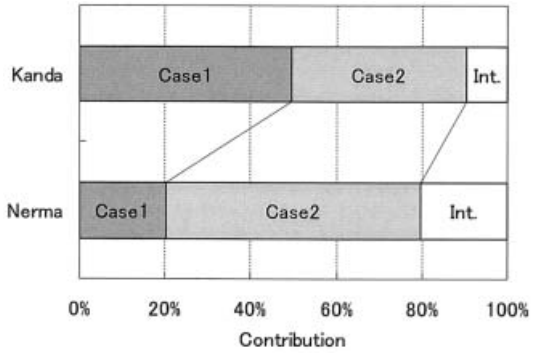

Fig. 19. Contribution of sensible heat release from building surfaces (Case1), wind reduction due to drag (Case2) and their interaction (Int.).

7. Conclusions

A numerical simulation was carried out to estimate the individual contribution of factors for UHI formation (heat flux released from building surfaces, wind reduction due to drag and those interaction) to the variation of air temperature in urban (Kanda), and suburban (Nerima) areas using a one-dimensional CM combined with a MM. Before the estimation, the validation of the MM and the CM was done with a statistical approach. The results indicated that the performance of the MM is reasonable for calculating temperatures, and less reliable for calculating the wind speed. On the other hand, the CM performance was fairly improved in predicting both temperature and wind speed. In addition, simultaneous measurements were conducted at two locations in Tokyo for a comparison between the results from the CM and those obtained from observations. The comparison indicated that the calculated temperatures in the Kanda and Nerima areas were closely predicted. However, nighttime temperature tends to be higher than the actual observation temperature. Finally, the individual contribution of each factor for UHI is estimated. The simulation results indicated that, in a comparison with the temperature of no building case (Case 3), the contribution of (i) heat flux released from building surfaces (Case1) was 49% in Kanda and 20% in Nerima, (ii) wind reduction due to drag (Case2) was 41% in Kanda and 59% in Nerima, and (iii) the effect of the interaction between Case1 and Case2 was +10% in Kanda and +20% in Nerima.

Acknowledgements

The authors thank Messrs. Katsuhiko Mutoh and Atsushi Takai of the National Institute of Advanced Industrial Science and Technology (AIST), Japan, for assisting with the observations, and Dr. Yukitaka Ohashi of the Okayama University of Science, Japan, for providing us useful advice. This study was supported by the Japanese Ministry of Environment.

References

Ando, H., T. Shioda, W. Morishima, S. Kojima, K. Ishii, T. Izumi, and T. Mikami, 2003: Spatial structure of summer temperatures over the urban area of Tokyo in 2002. *Annual report of Tokyo Metropolitan Research Institute for Environmental Protection*, 81–87.

Gambo, K., 1978: Notes on the turbulence closer model of atmospheric boundary layers. *J. Meteor. Soc. Japan*, **56**, 466–480.

Ichinose, T., K. Shimodozono, and K. Hanaki, 1999: Impact of anthropogenic heat on urban climate in Tokyo. *Atmos. Environ.*, **33**, 3897–3909.

JMA, 2002: Outline of the Operational Numerical Weather Prediction at the Japan meteorological Agency, Appendix to WMO Numerical Weather Prediction Progress Report. (http://www.jma.go.jp//jma/jma-eng/jma-center/nwp/outline-nwp/index.htm)

Jurges, W., 1924: Der Warmeuberergang an einer ebenen Wand. *Gesundeight-Ingnierur*, **19**, 1 (in German).

Keyser, D. and R.A. Anthes, 1977: The applicability of a mixed-layer model of the planetary boundary layer to real-data forecasting. *Mon. Wea. Rev.*, **105**, 1351–1371.

Kikegawa, Y., 2001: Evaluation of countermeasures against urban warming phenomena considering interaction between an urban thermal environment and air-conditioning energy demands. (Doctoral thesis, University of Tokyo) 205 pp. (in Japanese).

Kondo, J. (ed.), 1994: *The meteorology in a water environment*. Asakura-shoten, 350 pp. (in Japanese).

Kondo, H., 1989: Description of NRIPR mesoscale model. *Technical report No. 44, National Research Institute for Pollution and Resources*, 76 pp.

———, Y. Genchi, Y. Kikegawa, Y. Ohashi, H. Yoshikado, and H. Komiyama, 2005: Development of

a multi-layer urban canopy model for the analysis of energy consumption in a big city: Structure of the urban canopy model and its basic performance. *Bound.-Layer Meteor.*, **116**, 395–421.

——— and F.H. Liu, 1998: A study on the urban thermal environment obtained through a one-dimensional urban canopy model. *J. Jpn. Soc. Atmos. Environ.*, **33**, 179–192. (in Japanese).

Kusaka, H. and F. Kimura, 2004: Thermal Effects of Urban Canyon Structure on the Nocturnal Heat Island: Numerical Experiment Using a Mesoscale Model Coupled with an Urban Canopy Model. *J. Appl. Meteor.*, **43**, 1899–1910.

Martilli, A., 2002: Numerical Study of Urban Impact on Boundary Layer Structure: Sensitivity to Wind Speed Urban Morphology, and Rural Soil Moisture. *J. Appl. Meteor.*, **41**, 1247–1266.

Mikami, T., H. Ando, H. Yokoyama, T. Yamaguchi, K. Ishii, T. Shioda, W. Morishima, S. Kojima, and T. Izumi, 2004: Spatiotemporal variations of summer urban heat islands in Tokyo. *Annual report of Tokyo Metropolitan Research Institute for Environmental Protection*, 11–17.

Ohashi, Y., et al., 2005: Influence of air-conditioning waste heat on air temperature at the Tokyo office area during summer season—Numerical experiments using the urban canopy model coupled with the building energy model—. *J. Appl. Meteor. (accepted).*

———, Y. Genchi, and Y. Kikegawa, 2003: Horizontal distribution of surface air-temperature within urban district at the Tokyo central area and its formation factors. *J. Environ. Info. Sci.*, **17**, 59–64. (in Japanese).

Otte, T., A. Lacser, S. Dupont, and J.K.S. Ching, 2004: Implementation of an urban canopy parameterization in a meso-scale meteorological model. *J. Appl. Meteor.*, **43**, 1648–1665.

Pielke, R.A. and Y. Marher, 1978: Verification analysis of the University of Virginia three-dimensional meso-scale model prediction over south Florida for July 1, 1973. *Mon. Wea. Rev.*, **106**, 1568–1589.

Stein, U. and P. Alpert, 1993: Factor Separation in Numerical Simulations. *J. Atoms. Sci.*, **50**, 2107–2115.

Willmott, C.J., 1982: Some comments on the evaluation of model performance. *Bull. Amer. Meteor. Soc.*, **63**, 1309–1313.

Yoshikado, H., 1991: Relationship between hourly sunshine rate from the AMeDAS and global solar radiation. *Pollution Control*, **26**(1), 1–8. (in Japanese).